

# Study on Radiation Shielding Characteristics of Refractory High Entropy Alloys by EpiXS Code

Z. AYGUN\*

*Bitlis Eren University, Vocational School of Technical Sciences, 13100, Bitlis, Turkey*

Received: 30.10.2022 & Accepted: 05.12.2022

Doi: [10.12693/APhysPolA.143.66](https://doi.org/10.12693/APhysPolA.143.66)

\*e-mail: [zeynep.yarbasi@gmail.com](mailto:zeynep.yarbasi@gmail.com)

Refractory high entropy alloys constituted of refractory alloying elements, such as W, Zr, Nb, Ti, Mo, Ta, and Hf, are of great interest due to their widespread use in areas such as the defense, aerospace, and nuclear power generation industries. Refractory high entropy alloys are one of the subgroups of high entropy alloys and are evaluated as great candidates for replacements of superalloys commonly used at high temperatures due to their good mechanical properties and corrosion and oxidation resistance at high temperatures. The motivation for performing this study is that there is currently no comprehensive analysis of the radiation shielding abilities of this new type of high entropy alloys. The purpose of the study was to evaluate the radiation attenuation parameters such as mass and linear attenuation coefficients, half value layer, mean free path, effective atomic number, and buildup factors of the refractory high entropy alloys,  $\text{Al}_{0.5}\text{Mo}_{0.5}\text{NbTa}_{0.5}\text{TiZr}$ ,  $\text{Al}_{0.25}\text{NbTaTiZr}$ ,  $\text{HfMoScTaZr}$ ,  $\text{Nb}_{40}\text{Ti}_{25}\text{Al}_{15}\text{V}_{10}\text{Ta}_5\text{Hf}_3\text{W}_2$ ,  $\text{NbCrMo}_{0.5}\text{Ta}_{0.5}\text{TiZr}$ ,  $\text{Ti}_2\text{VNbMoZr}$ , and  $\text{W}_{23}\text{Mo}_{23}\text{V}_{17}\text{Cr}_8\text{Ta}_7\text{Fe}_{22}$  by using EpiXS software. The mass attenuation coefficients of the alloys were also calculated by XCOM, a well-known code, to see the consistency of the obtained values. It was concluded that  $\text{HfMoScTaZr}$  and  $\text{W}_{23}\text{Mo}_{23}\text{V}_{17}\text{Cr}_8\text{Ta}_7\text{Fe}_{22}$  have more shielding features, while  $\text{Ti}_2\text{VNbMoZr}$  has the lowest shielding ability among the alloys.

topics: radiation attenuation parameters, RHEAs, radiation shielding

## 1. Introduction

High entropy alloys (HEAs) are next-generation alloy systems that exhibit perfect mechanical, thermal, and chemical properties compared to most common alloys. HEAs have received great attention from researchers since first reported by Yeh et al. and Cantor et al. [1, 2] and can be divided into subgroups according to their application areas. One of these alloy groups is refractory high entropy alloy (RHEA), and it has been first reported by Senkov et al. [3]. Nine refractory elements (Mo, Nb, Ta, W, V, Hf, Zr, Ti, and Cr) with high melting points form the basis of RHEAs. [3, 4–8]. This new class HEA has importance and wide application areas in the aerospace industry [9, 10], the nuclear industry [11], the chemical process industry [5], and next-generation nuclear reactors due to its excellent oxidation and corrosion resistance, mechanical properties, and wear behavior even at high temperatures [12]. Especially for the aerospace industry, it is significant to improve the resistance of lightweight and high-strength materials against harsh environmental conditions. The density of RHEAs can be decreased by exchanging heavy refractory elements such as tungsten, molybdenum, hafnium,

and tantalum with lighter refractory elements [13]. Therefore, Zr, Nb, Mo, Ti, Cr, and V refractory metal elements with their low densities are preferred in the design of RHEAs. Researchers have developed new RHEAs for the advancement of the alloys also by adding Sc, Al, etc., which increase the plasticity and strength of the alloy [14–17].

The alloys used in reactor environments and nuclear applications have been widely investigated previously for their radiation shielding capabilities [18–20]. However, the radiation protection potentials of this new class of HEAs, called RHEAs, have not been studied in detail yet. The motivation of having knowledge about radiation shielding features of the RHEAs is significant and essential to fill this gap in the literature. An accurate evaluation of radiation–matter interaction parameters is necessary to provide relevant information. The value of the mass attenuation coefficient of the material indicates the probability of photon interaction and thus gives us an idea about the absorption potential of the material. The half value layer (HVL) is the thickness-related parameter used in designing and choosing any radiation attenuation material by halving the photon intensity. It is desirable for the material to have a lower HVL value. The effective

atomic number is the average atomic number of the material containing multiple elements and is used for the calculation of energy absorption and buildup factor when designing a radiation shield. The parameter can be used to obtain basic information about the chemical composition of the material. For instance, materials with lower effective atomic numbers ( $\leq 10$ ) may be organic substances, and inorganic compounds or metals have higher effective atomic numbers [21]. The buildup factor is significant in radiation shielding design and dosimetry applications. The effective dose to be given to the material and exposure of the material to photons can be estimated by energy absorption and exposure buildup factors. Estimation of the parameters is important to develop appropriate materials for different areas such as medical physics, agriculture, nuclear industry, etc. In this context, for the purpose of learning about the radiation protection abilities of the alloys, photon attenuation parameters such as mass attenuation coefficients (MAC), linear attenuation coefficients (LAC), effective atomic numbers ( $Z_{eff}$ ), mean free paths (MFP), half-value layers (HVL), exposure and energy absorption buildup factors (EBF and EABF) of new class RHEAs ( $Al_{0.5}Mo_{0.5}NbTa_{0.5}TiZr$ -S1,  $Al_{0.25}NbTaTiZr$ -S2,  $HfMoScTaZr$ -S3,  $Nb_{40}Ti_{25}Al_{15}V_{10}Ta_5Hf_3W_2$ -S4,  $NbCrMo_{0.5}Ta_{0.5}TiZr$ -S5,  $Ti_2VNbMoZr$ -S6, and  $W_{23}Mo_{23}V_{17}Cr_8Ta_7Fe_{22}$ -S7) were determined by EpiXS [22]. The windows-based application software is one of the recently developed user-friendly programs and is based on EPICS2017 of ENDF/B-VIII and EPDL97 of ENDF/B-VI.8. EpiXS was produced for photon attenuation, dosimetry, and shielding, which covers a broad energy range 1 keV–1 GeV. EpiXS has been a code widely preferred by researchers lately [19, 23–26]. The XCOM software [27] was developed in order to estimate MAC values or photon interaction cross-sections of a single element, compound, or composite mixture in a wide energy region of 1 keV–100 GeV. Recently, many researchers have used the XCOM code for the purpose of calculating the MAC values of the shielding materials [18, 28–30].

## 2. Materials and methods

In the study, the chemical compositions of the alloys were taken from the literature [13–15, 31–33] and are given in Table I.

The MAC corresponds to the interaction possibility between the mass per unit area of the material and photons, and can be obtained by the Beer–Lambert as given by

$$I = I_0 e^{-\mu t}, \quad (1)$$

$$\mu_m = \frac{\mu}{\rho} = \frac{\ln(I_0/I)}{\rho t} = \frac{\ln(I_0/I)}{t_m}, \quad (2)$$

where  $\mu_m$  [ $cm^2/g$ ] and  $\mu$  [ $cm^{-1}$ ] are mass and linear attenuation coefficients, respectively.

TABLE I

Chemical compositions of the studied RHEAs.

Sample/Sample code	$Al_{0.5}Mo_{0.5}NbTa_{0.5}TiZr/S1$	$Al_{0.25}NbTaTiZr/S2$	$HfMoScTaZr/S3$	$Nb_{40}Ti_{25}Al_{15}V_{10}Ta_5Hf_3W_2/S4$	$NbCrMo_{0.5}Ta_{0.5}TiZr/S5$	$Ti_2VNbMoZr/S6$	$W_{23}Mo_{23}V_{17}Cr_8Ta_7Fe_{22}/S7$
Mo	11.20	–	15.83	–	11.06	17.50	23.00
Fe	–	–	–	–	–	–	22.00
Nb	24.50	26.00	–	40.00	23.30	18.80	–
Ta	13.60	28.90	18.97	5.00	24.64	–	7.000
Ti	21.40	21.10	–	25.00	10.67	30.40	–
Zr	19.50	19.00	16.95	–	19.36	17.80	–
V	–	–	–	10.00	–	15.40	17.00
Hf	–	–	28.73	3.00	–	–	–
Al	9.80	5.00	–	15.00	–	–	–
Sc	–	–	19.55	–	–	–	–
W	–	–	–	2.00	–	–	23.00
Cr	–	–	–	–	10.98	–	8.00
Density	7.96	9.27	9.34	7.29	8.23	6.760	12.54

We can obtain MAC for any compound as follows [34]

$$\mu/\rho = \sum_i w_i (\mu/\rho)_i, \quad (3)$$

where  $w_i$  and  $(\mu/\rho)_i$  are the weight fraction and MAC of  $i$ -th constituent element, respectively.

Now,  $Z_{eff}$  can be calculated as

$$Z_{eff} = \frac{\sigma_T}{\sigma_e}, \quad (4)$$

where  $\sigma_e$  is the electronic cross-section and  $\sigma_T$  is the total atomic cross-section of any sample as given by [35]

$$\sigma_e = \sum_i \frac{1}{Z_i} f_i (\sigma_T)_i. \quad (5)$$

Here,  $f_i$  is the mole fraction of the  $i$ -th constituent element. An interpolation given by

$$Z_{eff} = \frac{Z_1 [\log(\sigma_2) - \log(\sigma_T)] + Z_2 [\log(\sigma_T) - \log(\sigma_1)]}{\log(\sigma_2) - \log(\sigma_1)} \quad (6)$$

can be also used for the explicit determination of  $Z_{eff}$ . In (6),  $\sigma_1$  and  $\sigma_2$  are the elemental cross-sections of two elements  $Z_1$  and  $Z_2$ .

The other parameters, HVL and MFP, important to analyze the shielding feature are determined by using  $\mu$  as follows

$$HVL = \frac{\ln(2)}{\mu}, \quad (7)$$

$$MFP = \frac{1}{\mu}. \quad (8)$$

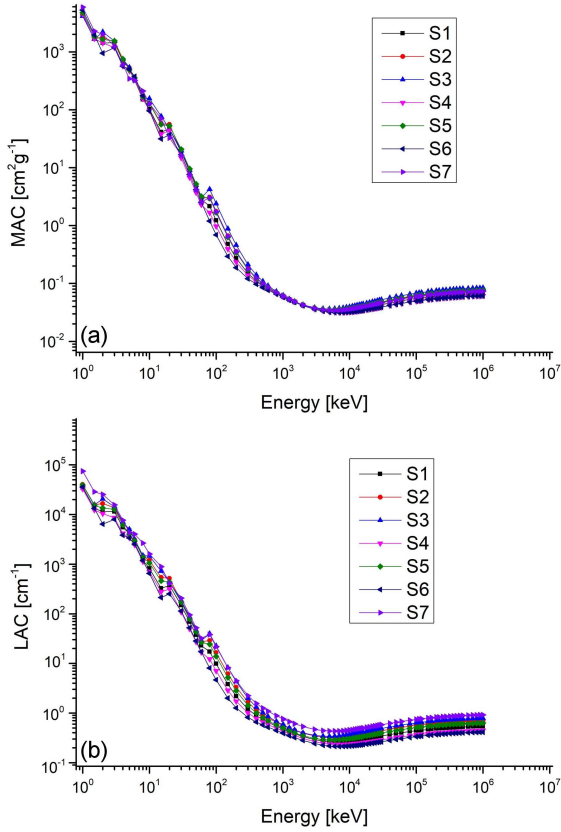


Fig. 1. The variations of MAC (a) and LAC (b) values versus photon energies.

EBF and EABF can be obtained using the equations given [36, 37]

$$Z_{\text{eq}} = \frac{Z_1[\log(R_2) - \log(R)] + Z_2[\log(R) - \log(R_1)]}{\log(R_2) - \log(R_1)}, \quad (9)$$

$$F = \frac{F_1[\log(Z_2) - \log(Z_{\text{eq}})] + F_2[\log(Z_{\text{eq}}) - \log(Z_1)]}{\log(Z_2) - \log(Z_1)}, \quad (10)$$

$$B(E, x) = 1 + \frac{(b-1)(K^x - 1)}{K - 1}, \quad \text{for } K \neq 1, \quad (11)$$

$$B(E, x) = 1 + (b-1)x, \quad \text{for } K = 1, \quad (12)$$

and

$$K(E, x) = cx^a + d \frac{\tanh\left(\frac{x}{X_k} - 2\right) - \tanh(-2)}{1 - \tanh(-2)} \quad (13)$$

for  $x \leq 40$  mfp.

The equivalent atomic number ( $Z_{\text{eq}}$ ) can be found by (9). The geometric progression (G-P) fitting parameters for the alloy are determined by using fitting parameters [38] in (10). Buildup factors can be obtained using (11) or (12) to determine  $K(E, x)$  in (13).

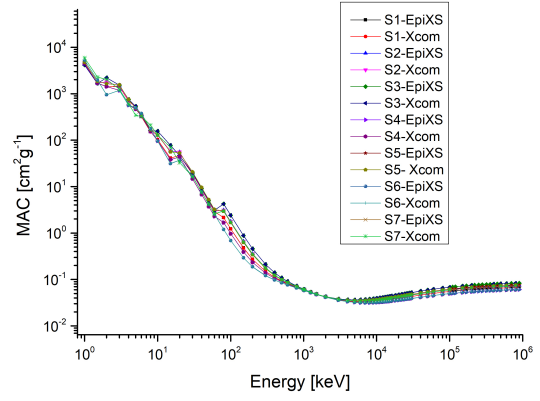


Fig. 2. The variations of MAC values of RHEAs versus photon energies determined using EpiXS and XCOM.

The ratio ( $R$ ) of Compton partial mass attenuation coefficient to total mass attenuation coefficient should be defined for the material at a specific energy. The  $R_1$  and  $R_2$  values indicate the  $(\mu_m)_{\text{Compton}}/(\mu_m)_{\text{total}}$  ratios of these two adjacent elements, which have  $Z_1$  and  $Z_2$  atomic numbers. In (10),  $F$  is the geometric progression fitting parameters ( $a, b, c, d, X_K$  coefficients) of the studied material, while  $F_1$  and  $F_2$  are the values of G-P fitting parameters identical with the  $Z_1$  and  $Z_2$  atomic numbers at a certain energy, respectively. In turn,  $E$  and  $x$  demonstrate primary photon energy and penetration depth, respectively. The combination of  $K(E, x)$  with  $x$  allows one to perform the photon dose multiplication and determine the shape of the spectrum.

### 3. Results and discussion

According to the chemical compositions of RHEAs (taken from the literature and given in Table I [13–15, 30–32]), and on the basis of knowledge about the alloys, the radiation–matter interaction parameters are determined. Changes in the calculated MAC values versus photon energies (1 keV–1 GeV) are presented in Fig. 1a. MAC values decreased sharply, slightly changed, and increased with increasing energy at, respectively, low (1–100 keV), mid (100 keV–5 MeV), and high (> 5 MeV) energies, where the photoelectric, the Compton scattering, and pair production processes are effective, respectively. The MAC values of the RHEAs were also determined by XCOM in order to investigate the compatibility of the obtained MAC results by EpiXS (Fig. 2). The small increase observed at 0.02 MeV can be due to the K-absorption edges of Mo, which was also reported by Sayyed et al. [20] for some alloys. The order of the MAC values at the same energy is  $S3 > S7 > S2 > S5 > S1 > S4 > S6$ . The MAC values of the RHEAs and previously reported superalloys for some energy values are given in Table II.

Comparison of the MAC values of the RHEAs and previously reported alloys.

TABLE II

Energy [MeV]	S1	S2	S3	S4	S5	S6	S7	Rene 41 [18]	Rene 77 [18]	Rene 80 [18]	Rene 95 [18]	Inc 617 [19]	Inc 800HT [19]	In 625 [20]	In 718 [20]
0.015	41.06	58.10	77.14	38.07	55.79	31.39	70.67	58.48	59.63	64.38	63.06	59.14	60.60	65.70	59.00
0.03	18.70	19.10	19.71	14.83	20.78	16.76	16.50	10.69	9.734	10.44	10.83	10.83	8.763	9.549	10.41
0.05	4.69	4.82	5.01	3.72	5.227	4.172	4.161	2.594	2.351	2.537	2.633	2.626	2.101	2.287	2.51
0.8	0.068	0.070	0.072	0.068	0.069	0.066	0.070	0.068	0.068	0.068	0.068	0.068	0.067	0.068	0.067
1	0.060	0.061	0.062	0.060	0.060	0.058	0.061	0.060	0.061	0.061	0.061	0.060	0.060	0.061	0.060
3	0.037	0.037	0.038	0.036	0.037	0.036	0.037	0.037	0.037	0.037	0.037	0.037	0.036	0.037	0.037
5	0.034	0.035	0.036	0.032	0.035	0.032	0.035	0.032	0.032	0.033	0.033	0.032	0.032	0.032	0.032
8	0.034	0.036	0.038	0.032	0.036	0.032	0.035	0.031	0.031	0.031	0.032	0.031	0.030	0.031	0.031
10	0.034	0.037	0.039	0.032	0.037	0.032	0.036	0.031	0.031	0.031	0.031	0.031	0.030	0.031	0.031

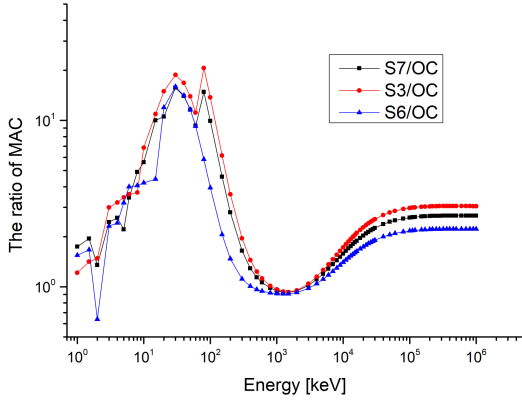


Fig. 3. The ratio of MAC values of S3, S6, and S7 to OC as reference material.

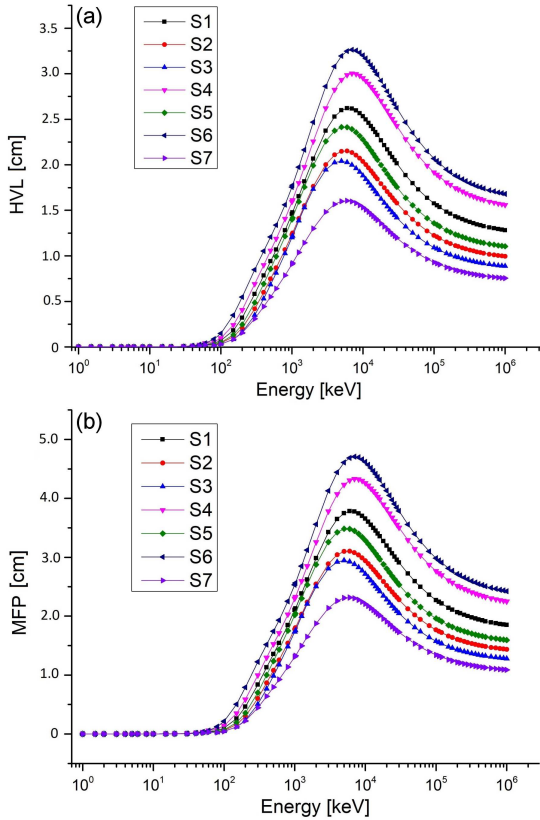


Fig. 4. The variations of HVL (a) and MFP (b) values versus photon energies.

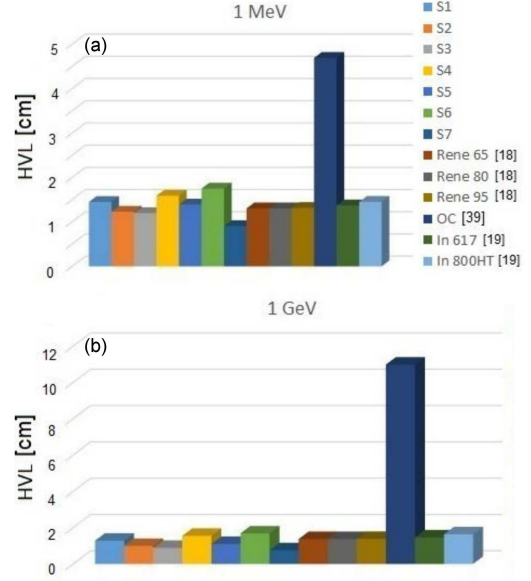


Fig. 5. Comparison of HVL values of the RHEAs with those of other previously studied materials.

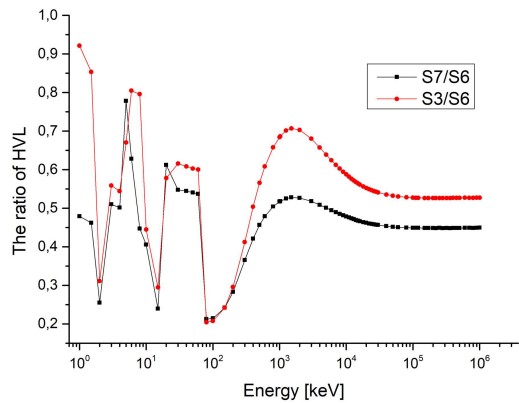


Fig. 6. The ratio of HVL values of S3 and S7 to S6.

The ratio of MAC values of RHEAs with the highest shielding properties (S7 and S3) and RHEA with the lowest one (S6) to other reference material, ordinary concrete (OC) [39], a widely used shielding material, is shown in Fig. 3. It is obvious that the MAC values of S3 are higher than S7 for the energies > 10 keV.

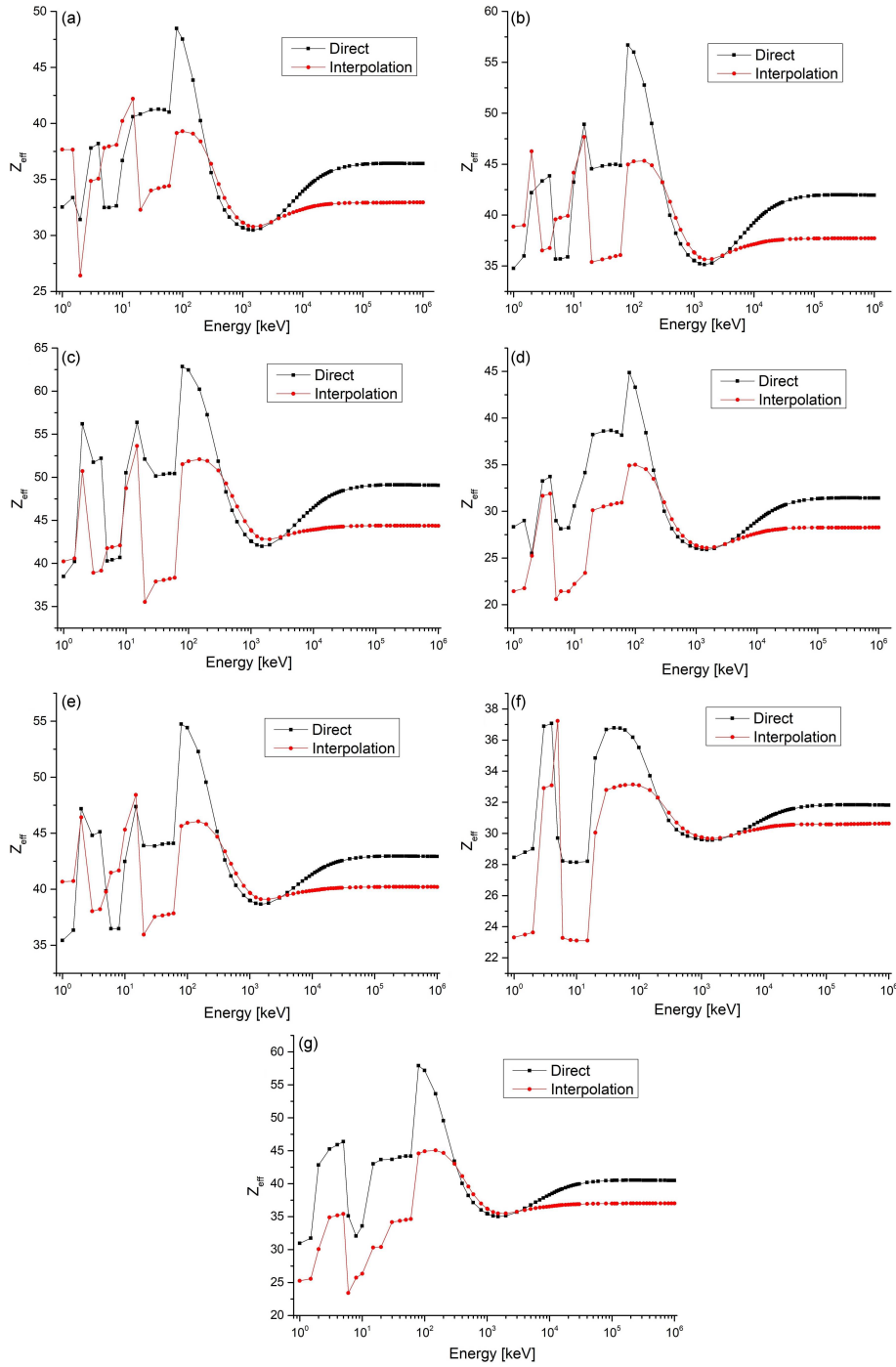


Fig. 7. The variations of  $Z_{\text{eff}}$  values of S1 (a) S2 (b) S3 (c) S4 (d) S5 (e) S6 (f) S7 (g) versus photon energies.

Variation of the calculated LAC values versus photon energies (1 keV–1 GeV) is shown in Fig. 1b. LAC is one of the parameters for defining the photon-matter interaction, and it is used to obtain MAC, HVL, and MFP shielding parameters. The value of LAC depends on both MAC and the density of the compound. The density effect causes greater differences for LAC values compared with MAC values. The highest LAC value among the alloys is seen for S3, while, at the same energy, the lowest is observed for S6.

HVL and MFP are other parameters for determining shielding abilities. HVL and MFP values changing versus photon energies determined by EpiXS are given in Fig. 4. At mid-energies, where Compton scattering is dominant, most photons are more likely to be scattered. Therefore, their absorption probabilities are lower, and hence thicker materials are required, and photons have longer MFP. It is preferred to have low HVL and MFP values in the high-energy regions for better-shielding properties. The order of the HVL values in the same energy

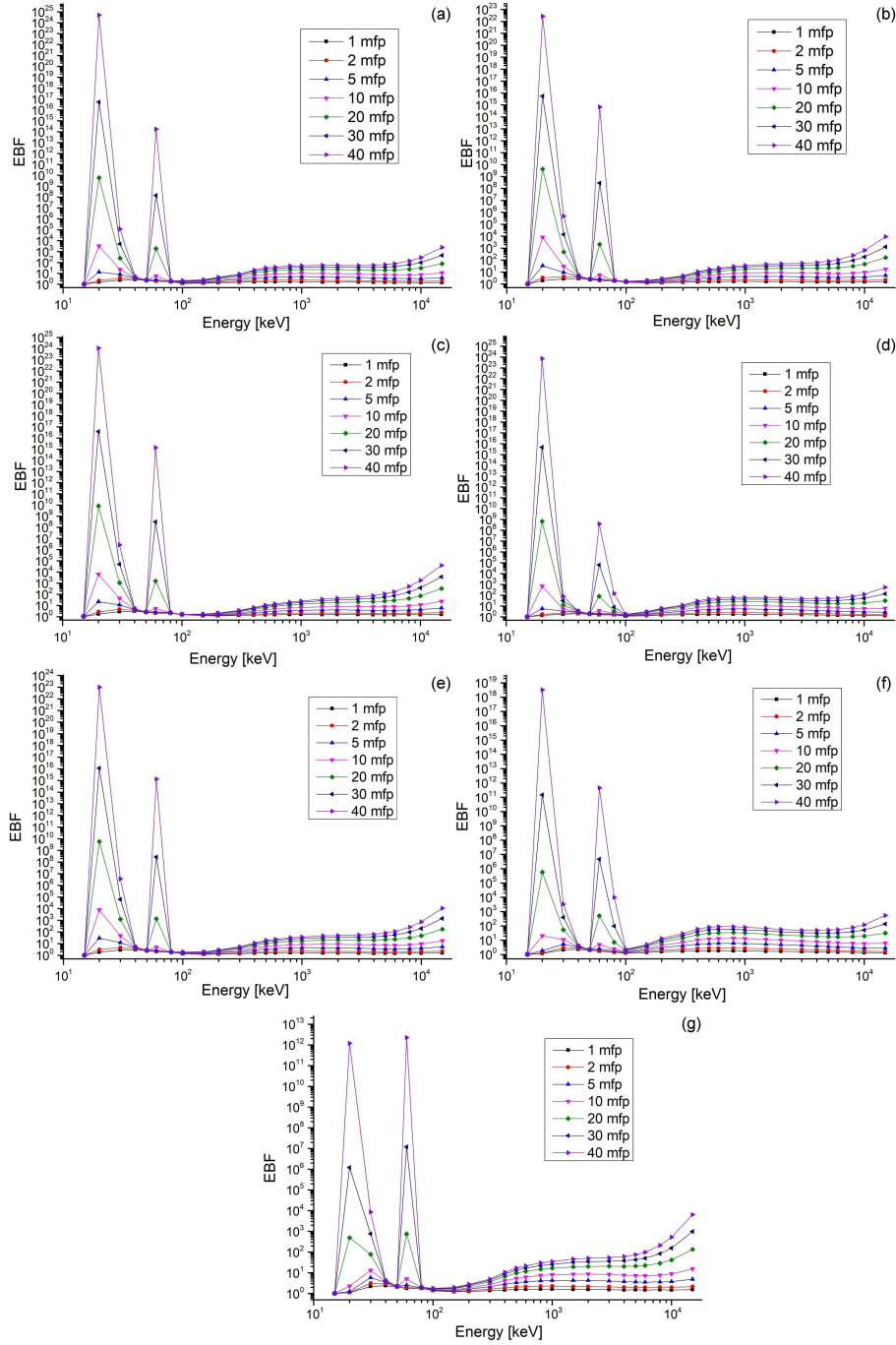


Fig. 8. The variations of EBF values of S1 (a) S2 (b) S3 (c) S4 (d) S5 (e) S6 (f) S7 (g) versus photon energies.

region is  $S6 > S4 > S1 > S5 > S2 > S3 > S7$ . The decreasing order of the MFP values in the same energy region is  $S6 > S4 > S1 > S5 > S2 > S3 > S7$ . According to the obtained results, HVL and MFP values of the alloy  $W_{23}Mo_{23}V_{17}Cr_8Ta_7Fe_{22}$  are lower than those of other alloys.  $Ti_2VNbMoZr$  alloy has the highest values of HVL and MFP. Therefore, it can be concluded that  $W_{23}Mo_{23}V_{17}Cr_8Ta_7Fe_{22}$  has a higher shielding ability than other studied alloys. In order to evaluate the shielding capacity of the RHEAs, the HVL values for two energies are compared with those of previously studied materials and

given in Fig. 5. The ratio of HVL values of the RHEAs with the highest shielding properties (S3 and S7) to the RHEA with the lowest one (S6) is shown in Fig. 6. It can be clearly seen that the ratio of HVL values for S7 are lower than that for S3, therefore, based on HVL values, S7 has a higher shielding ability than S3.

The variations of  $Z_{eff}$  versus photon energies obtained by the code are given in Fig. 7. At low energies, due to the photoelectric effect, maximum  $Z_{eff}$  values were obtained. The first maximum  $Z_{eff}$  at around 0.0015 MeV can be obtained by the

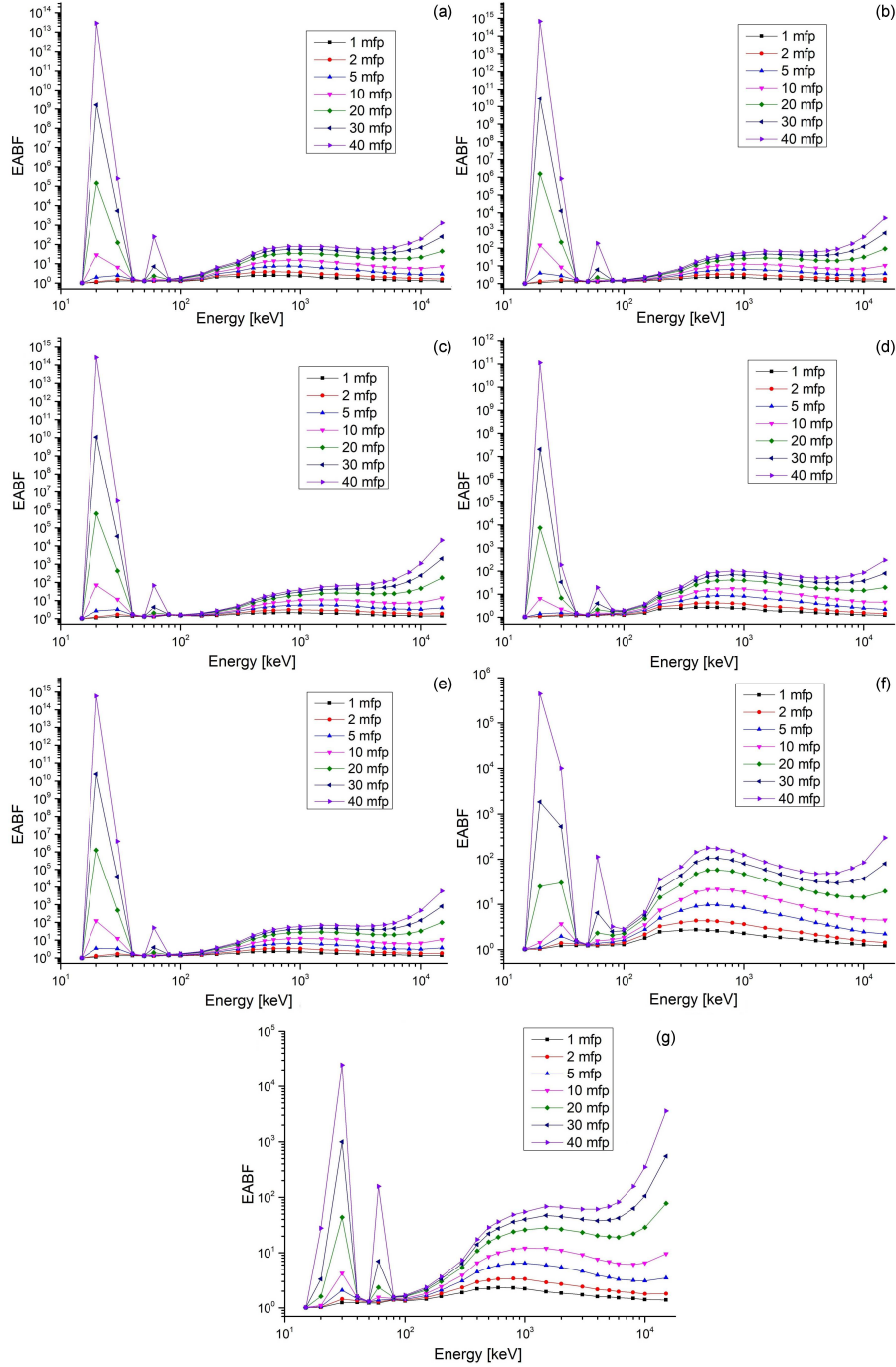


Fig. 9. The variations of EABF values of S1 (a) S2 (b) S3 (c) S4 (d) S5 (e) S6 (f) S7 (g) versus photon energies.

K-absorption edge of Al [40]. K-absorption edge of Zr with 0.018 MeV is observed for  $Z_{\text{eff}}$ , as seen in Fig. 7. The other maximum  $Z_{\text{eff}}$  values at around 0.019 and 0.02 MeV may be due to K-absorption edges of Nb and Mo, respectively [20]. These values decreased sharply with increasing energy. Then the values increased and remained stable at high energies. Among the RHE alloys, maximum  $Z_{\text{eff}}$  values are achieved for  $W_{23}Mo_{23}V_{17}Cr_8Ta_7Fe_{22}$  and  $HfMoScTaZr$  with the contribution of W, Ta, Hf, Zr, and Mo (higher atomic number), whereas

minimum  $Z_{\text{eff}}$  value is observed for  $Ti_2VNbMoZr$  with no contribution of Ta, Hf, and W. Due to the higher  $Z_{\text{eff}}$  values,  $W_{23}Mo_{23}V_{17}Cr_8Ta_7Fe_{22}$  and  $HfMoScTaZr$  alloys show higher shielding potential.  $Ti_2VNbMoZr$  has the lowest  $Z_{\text{eff}}$  value and so the lowest shielding property.

EABF and EBF of the alloys were determined for 7 penetration depths by EpiXS. The dependence of EABF and EBF versus incident photon energies is shown in Figs. 8 and 9. EABF and EBF reach the maximum at mid-energies. Maximum number of

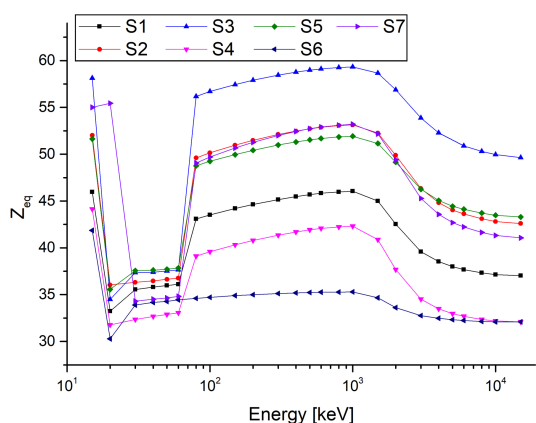


Fig. 10. The variations of  $Z_{eq}$  values of the alloys versus photon energies.

photons will be absorbed due to the photoelectric effect; therefore, buildup factor values are small at low photon energies. In the mid-energy region, the dominant process is Compton scattering. In the Compton region, an increase in photon accumulation is observed due to a large number of scattered photons, and hence EABF and EBF have great values at medium energies. At high energies, pair production is dominant, and a strong photon absorption is observed. As a result, the buildup factors decrease at high energies [19, 41]. Buildup factors decrease slowly with increasing photon energy ( $> 1500$  keV). This case may be due to the photons which can create electron-positron pairs with low kinetic energy. For energies greater than 8000 keV, the increase in the values of EABF and EBF is bigger in the higher-energy region at penetration depths of 20, 30, and 40 mfp [20]. The obtained values of EABF and EBF show that the lowest photons cluster is observed for  $W_{23}Mo_{23}V_{17}Cr_8Ta_7Fe_{22}$  RHEA. As a result, it can be noted that  $W_{23}Mo_{23}V_{17}Cr_8Ta_7Fe_{22}$  is the alloy in which the Compton scattering effect is most often observed. The first maximum at around 0.02 MeV may be due to the K-absorption edge of Mo, whereas the maximum seen at  $\approx 0.07$  MeV may be due to the K-absorption edge of W [20].

Equivalent atomic number ( $Z_{eq}$ ) is an effective parameter in determining energy absorption and absorbed dose. While all partial photon interactions are effective in the determination of  $Z_{eff}$ ,  $Z_{eq}$  is calculated only by Compton scattering [42]. The calculated  $Z_{eq}$  of the alloys are given in Fig. 10. It was established that  $Z_{eq}$  values of  $W_{23}Mo_{23}V_{17}Cr_8Ta_7Fe_{22}$  and  $HfMoScTaZr$  are higher than those of other alloys.

#### 4. Conclusions

In the study, radiation-matter interaction parameters of RHEAs were calculated using EpiXS code in the range of 1 keV–1 GeV in order to determine the radiation protection abilities. MAC

was also determined by using XCOM, and it has been found that the obtained results are in good agreement. It can also be mentioned that  $W_{23}Mo_{23}V_{17}Cr_8Ta_7Fe_{22}$  and  $HfMoScTaZr$  show higher shielding capability than other RHEAs, while  $Ti_2VNbMoZr$  has the lowest shielding property among the alloys. It can be noted that having heavy metal (such as Hf, W, Ta, Mo, etc.) contents increase the radiation shielding ability of the alloys. It was also determined that the HVL values of the RHEAs are lower than those of previously studied materials such as traditional ordinary concrete and superalloys. Lastly, it is important to say that the studied RHEAs can be evaluated as new type shielding materials in the aerospace industry, nuclear industry, chemical process industry, and next-generation nuclear reactors due to their superior features.

#### References

- [1] B.J.W. Yeh, S.K. Chen, S.J. Lin, J.Y. Gan, T.S. Chin, T.T. Shun, C.H. Tsau, S.Y. Chang, *Adv. Eng. Mater.* **6**, 299 (2004).
- [2] B. Cantor, I.T.H. Chang, P. Knight, A.J.B. Vincent, *Mater. Sci. Eng. A* **213**, 375 (2004).
- [3] O.N. Senkov, G.B. Wilks, D.B. Miracle, C.P. Chuang, P.K. Liaw, *Intermetallics* **18**, 1758 (2010).
- [4] D. Miracle, O. Senkov, *Acta Materialia* **122**, 448 (2017).
- [5] O.N. Senkov, D.B. Miracle, K.J. Chaput, J.P. Couzinie, *J. Mater. Res.* **33**(19), 3092 (2018).
- [6] C.H. Chang, M.S. Titus, J.W. Yeh, *Adv. Eng. Mater.* **20**, 1700948 (2018).
- [7] N. Yurchenko, E. Panina, S. Zhrebtsov, G. Salishchev, N. Stepanov, *Materials* **11**, 2526 (2018).
- [8] B. Gorr, F. Müller, M. Azim, H.J. Christ, T. Müller, H. Chen, A. Kauffmann, M. Heilmaier, *Oxid. Met.* **88**, 339 (2017).
- [9] Y. Ye, Q. Wang, J. Lu, C. Liu, Y. Yang, *Mater. Today* **19**, 349 (2016).
- [10] T. Dam, S. Shaba, B.A. Thesis, Chalmers University of Technology, 2016.
- [11] A. Kareer, J.C. Waite, B. Li, A. Couet, D.E.J. Armstrong, A.J. Wilkinson, *J. Nucl. Mater.* **526**, 151744 (2019).
- [12] A. Ayrenk, M.Sc Thesis, Cankaya University, 2020.
- [13] T. Li, J. Miao, Y. Lu, T. Wang, T. Li, *Int. J. Refract. Metals Hard Mater.* **103**, 105762 (2022).
- [14] X.W. Nie, M.D. Cai, S. Cai, *Int. J. Refract. Metals Hard Mater.* **98**, 105568 (2021).

- [15] J. Pang, H. Zhang, L. Zhang, Z. Zhu, H. Fu, F. Li, A. Wang, Z. Li, H. Zhang, *Mater. Sci. Eng. A* **831**, 142290 (2022).
- [16] Y. Cao, Y. Liu, B. Liu, W. Zhang, J. Wang, M. Du, *Trans. Nonferrous Met. Soc. China* **29**, 1476 (2019).
- [17] V. Bhardwaj, Q. Zhou, F. Zhang, W. Han, Y. Du, K. Hua, H. Wang, *Tribol. Int.* **160**, 107031 (2021).
- [18] Z. Aygun, M. Aygun, *Acta Phys. Pol. A* **141**, 507 (2022).
- [19] Z. Aygun, M. Aygun, *J. Polytech.*, 1-1 (2022) (in press).
- [20] M.I. Sayyed, F.Q. Mohammed, K.A. Mahmoud, E. Lacomme, K.M. Kaky, M.U. Khandaker, M.R.I. Faruque, *Appl. Sci.* **10**, 7680 (2020).
- [21] M.I. Sayyed, S.A.M. Issa, S.H. Auda, *Progress Nucl. Energy* **100**, 297 (2017).
- [22] F.C. Hila, A.A. Astronomo, C.A.M. Dingle et al., *Radiat. Phys. Chem.* **182**, 109331 (2021).
- [23] M.B.Z. Gili, J.F.M. Jecong, *Arab. J. Sci. Eng.* **48**, 1021 (2022).
- [24] N. Arpac, M. Aygun, *J. Amasya Univ. Inst. Sci. Technol.* **3**, 8 (2022).
- [25] H. Akhdar, *Nanomaterials* **12**, 3577 (2022).
- [26] Z. Aygun, M. Aygun, N. Yarbasi, *J. New Results Sci.* **10**, 46 (2021).
- [27] M.J. Berger, J.H. Hubbell, *XCOM: Photon Cross Sections Database, Web Version 1.2*, National Institute of Standards and Technology, Gaithersburg (MD) 1987.
- [28] R. Kurtulus, T. Kavas, I. Akkurt, K. Gunoglu, H.O. Tekin, C. Kurtulus, *J. Mater. Sci. Mater. Electron.* **32**, 13882 (2021).
- [29] M.I. Sayyed, A.A. Ali, H.O. Tekin, Y.S. Rammah, *Appl. Phys. A* **125**, 445 (2019).
- [30] Y.S. Rammah, A.S. Abouhasw, A.H. Salam, R. El-Mallawany, *J. Theor. Appl. Phys.* **13**, 155 (2019).
- [31] O.N. Senkov, C.F. Woodward, *Mater. Sci. Eng. A* **529**, 311 (2011).
- [32] S. Das, P.S. Robi, *Int. J. Refract. Met. Hard Mater.* **100**, 105656 (2021).
- [33] O.N. Senkov, J.K. Jensen, A.L. Pilchak, D.B. Miracle, H.L. Fraser, *Mater. Design* **139**, 498 (2018).
- [34] D.F. Jackson, D.J. Hawkes, *Phys. Rep.* **70**, 169 (1981).
- [35] S.R. Manohara, S.M. Hanagodimath, *Nucl. Inst. Methods Phys. Res. B* **258**, 321 (2007).
- [36] Y. Harima, Y. Sakamoto, S. Tanaka, M. Kawai, *Nucl. Sci. Eng.* **94**, 24 (1986).
- [37] Y. Harima, *Radiat. Phys. Chem.* **41**, 631 (1993).
- [38] ANSI/ANS 6.4.3. "Gamma-Ray Attenuation Coefficients and Buildup Factors for Engineering Materials", American Nuclear Society, La Grange Park, (IL) 1991.
- [39] I.I. Bashter, *Ann. Nucl. Energy* **24**, 1389 (1997).
- [40] V.P. Singh, N.M. Badiger, T. Korkut, *Prog. Nucl. Energy* **104**, 1 (2018).
- [41] Z. Aygun, M. Aygun, *Int. J. Environ. Sci. Technol.* **19**, 5675 (2022).
- [42] Z. Aygun, N. Yarbasi, M. Aygun, *Ceram. Int.* **47**, 34207 (2021).